• Basic Research •

Depression induces ocular surface inflammation and dry eye-like changes in mice

Xiang Lin[1], Yu-Wen Liu[2], Jia-Ni Li[2], Wei-Jie Ouyang[2,3], Li-Ying Tang[2,4], Jie-Li Wu[2,5], Zhao-Lin Liu[2,6], Shi-Nan Wu[2], Jiao-Yue Hu[1,2], Zu-Guo Liu[2,6]

[1]Department of Ophthalmology, Xiang'an Hospital of Xiamen University; Eye Institute of Xiamen University; Fujian Provincial Key Laboratory of Ophthalmology and Visual Science; Fujian Engineering and Research Center of Eye Regenerative Medicine; School of Medicine, Xiamen University, Xiamen 361005, Fujian Province, China

[2]Xiamen Eye Center of Xiamen University, Fujian Provincial Key Laboratory of Ophthalmology and Visual Science, Fujian Engineering and Research Center of Eye Regenerative Medicine, Eye Institute of Xiamen University, School of Medicine of Xiamen University, Xiamen 361005, Fujian Province, China

[3]Department of Ophthalmology, the Affiliated Hospital of Guizhou Medical University, Guiyang 550004, Guizhou Province, China

[4]Department of Ophthalmology, Zhongshan Hospital, Xiamen University, Xiamen 361000, Fujian Province, China

[5]Aier Eye Hospital Group, Changsha 410015, Hunan Province, China

[6]Department of Ophthalmology, the First Affiliated Hospital of University of South China, Hengyang 421001, Hunan Province, China

Co-first Authors: Xiang Lin and Yu-Wen Liu

Correspondence to: Zu-Guo Liu and Jiao-Yue Hu. Xiang'an Campus of Xiamen University, 401, Chengyi Build, South Xiang-an Rd, Xiamen 361005, Fujian Province, China. zuguoliu@xmu.edu.cn; mydear_22000@163.com

Received: 2025-07-31 Accepted: 2025-10-17

Abstract

● **AIM:** To investigate the impact of depression-like behavior on ocular surface homeostasis in a mouse model, with a focus on dry eye-like alterations.

● **METHODS:** Male C57BL/6J mice (10–12 weeks old) were randomly assigned to control or restraint stress (RS) groups. The RS group underwent three intermittent 24-hour restraint sessions to induce depressive-like behavior. Behavioral testing, tear secretion measurement, and corneal Oregon Green Dextran (OGD) staining were performed. Postmortem analyses included histological evaluation of lacrimal glands, goblet cell quantification using periodic acid-Schiff staining, and assessment of key inflammatory and apoptotic markers: interleukin (IL)-17, matrix metalloproteinases (MMP)-3, MMP-9, IL-13, interferon (IFN)-γ, and cleaved caspase-3 and -8.

● **RESULTS:** Repeated RS induced depression-like behavior and significant ocular surface changes. RS-treated mice showed increased corneal OGD uptake and upregulation of gene/protein expression of IL-17, MMP-3, and MMP-9 (P<0.05). Goblet cell density and IL-13 protein expression were reduced, while IFN-γ protein expression was elevated (P<0.05). Cleaved caspase-3 and -8 levels were significantly increased in both cornea and conjunctiva. Tear volume and lacrimal gland size were unchanged; however, mild inflammatory infiltration was observed in lacrimal glands.

● **CONCLUSION:** Repeated RS leads to ocular surface inflammation and dry eye-like pathology, including corneal barrier disruption, goblet cell loss, and epithelial apoptosis. These findings suggest that depression contributes to the pathogenesis of dry eye disease *via* immune-mediated mechanisms.

● **KEYWORDS:** depression; restraint stress; dry eye; ocular surface damage; inflammation; mice

DOI:10.18240/ijo.2026.03.02

Citation: Lin X, Liu YW, Li JN, Ouyang WJ, Tang LY, Wu JL, Liu ZL, Wu SN, Hu JY, Liu ZG. Depression induces ocular surface inflammation and dry eye-like changes in mice. *Int J Ophthalmol* 2026;19(3):434-442

INTRODUCTION

Depression is a highly prevalent and debilitating mental disorder, affecting over 280 million people worldwide and ranking among the leading causes of disability (WHO, 2023)[1]. Beyond its well-documented impact on mental and systemic health, recent studies have revealed associations between depression and various ocular diseases, including glaucoma, age-related macular degeneration, and, most notably, dry eye disease (DED)[2-3].

DED is a chronic, multifactorial ocular surface disorder characterized by tear film instability, elevated tear osmolarity, and inflammatory processes, which collectively result in ocular discomfort, visual impairment, and epithelial damage[4]. Emerging epidemiological evidence reveals a complex bidirectional relationship between DED and depression. Patients with DED demonstrate a significantly higher prevalence of depressive symptoms compared to those with other ophthalmologic conditions, while individuals with depression exhibit objective alterations in tear film parameters[5-7]. Clinical studies have documented reduced tear film break-up time and diminished Schirmer test values in newly diagnosed depression patients relative to healthy controls[8-9]. Moreover, the co-occurrence of these conditions appears to have synergistic effects, with patients experiencing both DED and depression presenting with more severe ocular symptoms and pronounced clinical signs[5,10]. These convergent findings suggest that depression may contribute to DED pathogenesis through shared pathophysiological mechanisms, highlighting the need for comprehensive mechanistic investigations of this bidirectional association.

Despite the growing recognition of depression as a risk factor for DED, existing studies have predominantly focused on clinical associations or the ocular side effects of antidepressants. The underlying biological mechanisms by which depression contributes to ocular surface damage remain poorly understood. To address this gap, we established a repeated 24-hour restraint stress (RS) model to induce depression-like behaviors in mice and evaluated its impact on ocular surface integrity and inflammation. Specifically, we investigated corneal epithelial barrier integrity, goblet cell density, apoptosis markers, and lacrimal gland pathology.

MATERIALS AND METHODS

Ethical Approval All procedures involving animals were approved by the Animal Ethics Committee of Xiamen University (Approval No. IACUC-20190311-01) and adhered to the ARVO Statement for the Use of Animals in Ophthalmic and Vision Research.

Animal Model of Depression Male C57BL/6J mice (10–12 weeks old) were obtained from the Experimental Animal Center of Xiamen University. To minimize the impact of environmental variables on the ocular surface, we employed a 24-hour RS protocol to induce depression-like behaviors in mice, following a previously established method[11-12]. Male mice were randomly assigned to either the control (CTL) group or the RS group.

Mice in the CTL group were housed in individually ventilated cages (IVC) under standard environmental conditions: temperature 25℃±1℃, humidity 55%±15%, and a 12-hour light/dark cycle (lights on from 08:00 to 20:00; average light intensity ~300 lx). Background noise was maintained below 60 dB, and food and water were provided ad libitum.

In the RS group, mice were individually placed in 50 mL conical centrifuge tubes (Cat# 339652, ThermoFisher Scientific, Waltham, MA, USA) for 24h per session, from 08:00 to 08:00 the following day. The tubes were perforated with 5 mm ventilation holes to allow airflow and tail extension, while restricting movement and preventing rotation. During the restraint period, animals were deprived of food and water, kept in continuous darkness, and exposed to elevated background noise exceeding 80 dB, primarily from air-conditioning vents. After each restraint session, mice were returned to their original IVC cages under standard housing conditions for a 48-hour recovery period. This 24-hour RS and 48-hour recovery cycle was repeated three times (on days 1, 4, and 7). All subsequent experiments were performed starting on day 10.

Animal Behavior Test To confirm the development of depression-like behaviors following repeated RS, a series of behavioral tests were conducted, including the open field test (OFT), tail suspension test (TST), forced swim test (FST), and sucrose preference test (SPT). All behavior tests were conducted in a specialized behavior lab with ambient noise levels maintained below 40 dB. Before testing, mice were acclimated to the lab for at least 60min. Behavioral data were recorded and analyzed using the SMART video-tracking software system (Version 3.0.0.5; Harvard Apparatus; Holliston, MA, USA) and digital cameras positioned at different angles.

Open-field test OFT was performed in a white square open-field box (50 cm×50 cm×30 cm, ZH-SBS; Zhenghua Biotechnical Equipment Co., Ltd., Huaibei, Anhui Province, China), illuminated to 200 lx. The floor was divided into two equal areas: a central region and a distal region. Mice were placed in the center of the box and allowed to explore for 30s. The following parameters were recorded during the final 5min of the test using SMART software: total distance traveled, number of entries into the center region, time spent in the center region, and mean walking velocity. The box was cleaned with 70% ethanol between tests to prevent odor contamination.

Tail suspension test Mice were suspended by adhesive tape placed 1 cm from the tip of the tail, 50 cm above the floor. After 1min of acclimation, the mice were observed for 5min. The immobility time, defined as passive, motionless hanging, was recorded and analyzed by an observer blinded to the treatment group.

Forced swimming test FST was performed over two days. On day 1, mice were placed in a 2-L beaker filled with 1.8 L of water at 25℃±1℃. The mice were unable to climb out or touch the bottom. After 15min, the mice were dried and placed on a heated blanket to prevent hypothermia. On day 2, the

procedure was repeated for 5min. Behaviors were recorded using a high-definition camera. Immobility was defined as lack of movement throughout the body, with no hindlimb movement and minimal forelimb movement required to keep the head above water. A blinded observer analyzed the video recordings.

Sucrose preference test SPT was performed in the home cage using a two-bottle choice paradigm. Initially, two bottles of 1% sucrose solution were presented for 24h. Afterward, one bottle was replaced with tap water, and the positions of the bottles were switched once during the test. After 12h of water and food deprivation, mice were given free access to both bottles for 12h. The sucrose preference was calculated using the formula

$$\text{sucrose preference (\%)} = \frac{\text{sucrose intake (g)}}{\text{sucrose intake (g)} + \text{water intake (g)}} \times 100\%.$$

Histology The eyes and ocular adnexa, including eyelids and extraorbital lacrimal glands, were harvested for histological analysis. Tissues were fixed in 4% paraformaldehyde (PFA; Cat# P1110; Solarbio; Beijing, China) at 4℃ overnight, followed by dehydration through a graded ethanol series (70%, 80%, 95%, and 100%×3) and clearing in xylene (100%×3). Samples were then infiltrated with paraffin wax (Cat# P3683; Sigma-Aldrich; Saint Louis, MO, USA) at 60℃, embedded, and sectioned at a thickness of 5 μm. Sections were mounted onto microscope slides (Cat# 188105; CITOTEST Scientific; Jiangsu Province, China) at room temperature for hematoxylin and eosin (H&E) and periodic acid-Schiff (PAS) staining.

For immunofluorescence and immunohistochemistry, tissues were embedded in optimal cutting temperature (OCT) compound (Cat# 4583; Tissue-tek; Sakura Americas, Torrance, CA, USA), snap-frozen in liquid nitrogen and stored at -80℃. Serial sagittal sections (5 μm) were prepared using a cryostat (CM1950; Leica; Wetzlar, Germany) for subsequent immunofluorescence and CD4 immunohistochemistry staining.

Hematoxylin and eosin staining Paraffin-embedded lacrimal gland sections were dewaxed and rehydrated in decreasing concentrations of ethanol (100%, 95%, and 80%). The sections were then stained with 10% hematoxylin (Cat# GHS132; Sigma-Aldrich; Saint Louis, MO, USA) for 6min, followed by 1% eosin (Cat# HT110132; Sigma-Aldrich; Saint Louis, MO, USA) for 3min. After staining, the sections were dehydrated though graded ethanol (80%, 95%, and 100%) and xylene, and mounted with a neutral gum seal (Cat# G8590; Solarbio; Beijing, China). Images were captured using a Carl Zeiss light microscope (AXIO; Carl Zeiss; Oberkochen, Germany).

Immunofluorescent staining Immunofluorescence was performed as previously described[13]. Briefly, 5-μm thick ocular cryosections were fixed in pre-cooled acetone at -20℃ for 10min, permeabilized with 0.2% Triton X-100 for 20min, and blocked with 2% bovine serum albumin (BSA; Cat# A8020; Solarbio; Beijing, China) for 1h. Sections were then incubated overnight at 4℃ with primary antibodies: cleaved caspase-3 (1:400 dilution; Cat# 9661S; CST; Boston, MA, USA) and cleaved caspase-8 (1:800 dilution; Cat# 8592S; CST; Boston, MA, USA). Following primary antibody incubation, sections were incubated with Alexa Fluor 488 donkey anti-rabbit IgG (1:300 dilution; Cat# A21206; Invitrogen; Eugene, OR, USA) for 1h at room temperature. Nuclei were counterstained with 4',6-diamidino-2-phenylindole (DAPI; Invitrogen; Eugene, OR, USA). Fluorescence images were captured using a Leica fluorescent microscope (DFC7000 T; Leica; Wetzlar, Germany), and fluorescence intensity was analyzed with NIS-Elements software (Version 4.1; Nikon; Melville, NY, USA) according to the operating instructions of the software.

Tear Volume Measurement Tear volume was assessed on day 10 without anaesthetization. Phenol red-impregnated cotton threads (Zone-Quick; Yokota, Tokyo, Japan) were grasped using a micro-needle holder and placed in the inferior conjunctival sac at the lateral third of the lower eyelid in both eyes for 15s. The length of the moistened (red-stained) portion of the thread was measured in millimeter (mm) under an optical microscope (AXIO; Carl Zeiss; Oberkochen, Germany) by an investigator blinded to the experimental groups.

Corneal Epithelial Permeability Corneal epithelial barrier function was evaluated using Oregon Green Dextran (OGD; Cat# D7172; Invitrogen; Eugene, OR, USA). Briefly, after euthanasia, 0.5 μL of 50 mg/mL OGD solution was applied to the superficial central cornea of the right eye. After 1min, excess dye was rinsed off with 1 mL of saline five times. High-resolution fluorescent images were captured using a multi-zoom fluorescence microscope (AZ100; Nikon; Tokyo, Japan) equipped with a 470 nm laser used as the excitation light source. The fluorescence intensity within a 3-mm-diameter circular area of the central cornea was quantified using NIS-Elements software according to the operating instructions of the software.

Goblet Cell Density Conjunctival goblet cells were identified by PAS kit (Cat# 395B-1KT; Sigma-Aldrich; Saint Louis, MO, USA) according to manufacturer's instructions. Images were captured by an optical microscope equipped with an HD digital camera (AXIO; Carl Zeiss; Oberkochen, Germany). Goblet cells were manually counted by blinded observers. Goblet cell density was expressed as the number of PAS-positive cells per millimeter of conjunctival length, measured using NIS-Elements software.

RNA Extraction and Quantitative Reverse-Transcription PCR Total RNA was extracted from cornea and conjunctiva by using TRIZOL Reagent (Cat# 15596018; Invitrogen;

Table 1 Primer sequences used for quantitative qRT-PCR

Target gene	Forward	Reverse
MMP-3	CCTTTTGATGGGCCTGGAAC	GAGTGGCCAAGTTCATGAGC
MMP-9	CAATCCTTGCAATGTGGATG	AGTAAGGAAGGGGCCCTGTA
IL-17	CGCAATGAAGACCCTGATAGAT	CTCTTGCTGGATGAGAACAGAA
IL-13	GCAGCATGGTATGGAGTGT	TATCCTCTGGGTCCTGTAGATG
IFN-γ	AAATCCTGCAGAGCCAGATTAT	GCTGTTGCTGAAGAAGGTAGTA
β-actin	CCTAAGGCCAACCGTGAAAAG	AGGCATACAGGGACAGCACAG

qRT-PCR: Reverse-transcription polymerase chain reaction; MMP-3: Matrix metalloproteinase 3; MMP-9: Matrix metalloproteinase 9; IL-17: Interleukin 17; IL-13: Interleukin 13; IFN-γ: Interferon gamma.

Eugene, OR, USA) according to manufacturer's instructions which consisted of homogenization, phase separation, RNA precipitation, RNA wash and redissolving the RNA. RNA purity and concentration were assessed with a spectrophotometer (Nanodrop One/One^c; ThermoFisher Scientific; Waltham, MA, USA), with samples displaying an A260/280 ratio between 1.6 and 1.8 considered acceptable. A total of 1 μg of total RNA was then reverse-transcribed into cDNA using the RevertAid First Strand cDNA Synthesis kit (Cat# K1622; ThermoFisher Scientific; Waltham, MA, USA) in a 20 μL reaction volume. Quantitative reverse-transcription polymerase chain reaction (qRT-PCR) was performed using a LightCycler® 96 fluorescence quantitative PCR system (Roche; Penzberg, Germany) with SYBR Green Master Mix (Cat# 11201ES08; Yeasen; Shanghai, China) for amplification. Relative gene expression was calculated using the $2^{-\Delta\Delta Ct}$ method. Primer sequences were listed in Table 1, and all primers were synthesized by Sangon Biotech (Shanghai, China).

Western Blot Analysis Corneal and conjunctival tissues were homogenized in RIPA lysis buffer (Cat# 78440; ThermoFisher Scientific; Waltham, MA, USA) on ice. Lysates were centrifuged at 12 000 rpm for 15min at 4℃, and protein concentrations were determined using a BCA protein assay kit (Cat# 23227; ThermoFisher Scientific; Waltham, MA, USA). Equal amounts (30 μg) of protein were mixed with 4× DualColor protein loading buffer (Cat# AR1142; Boster Biological Technology; Wuhan, China), denatured at 100℃ for 10min, and stored at -80℃ until analysis. Proteins were separated by 10% or 12% SDS-PAGE and transferred to PVDF membranes (Cat# IPVH00010; Millipore, Billerica, MA, USA) under 90 V. Membranes were blocked in 5% skimmed milk for 1h and incubated overnight at 4℃ with primary antibodies against matrix metalloproteinases (MMP)-3 (1:1000 dilution; Cat# SC-6839; Santa Cruz; CA, USA), MMP-9 (1:1000 dilution; Cat# ab38898; Abcam; MA, USA), interleukin (IL)-17A (1:1000 dilution; Cat# ab79056; Abcam; MA, USA), interferon (IFN)-γ (1:1000 dilution; Cat# SC-12755; Santa Cruz; CA, USA), cleaved caspase-3 (1:1000 dilution; Cat# 9661S; CST; Boston, MA, USA) and cleaved-caspase-8 (1:1000 dilution; Cat# NB100-56116; Novus Biologicals; Littleton, CO). Appropriate HRP-conjugated secondary antibody goat anti-rabbit IgG (1:10 000 dilution; Cat# ab205718; Abcam; MA, USA) and rabbit anti-goat IgG (1:10 000 dilution; Cat# ab6741; Abcam; MA, USA) were incubated at room temperature for 1h. Immunoreactive bands were detected using enhanced chemiluminescence (ECL-500; Lulong Inc; Xiamen, China) and visualized with a Bio-Rad imaging system (734BR0275; Bio-Rad Laboratories; Hercules, CA, USA). Band intensities were quantified using Image Lab software (Version 4.1; Bio-Rad Laboratories; Hercules, CA, USA).

Enzyme-Linked Immunosorbent Assay Total conjunctival protein was homogenized in RIPA buffer, and concentrations were measured using a BCA protein assay kit as described above. The levels of IL-13 were measured by enzyme-linked immunosorbent assay (ELISA) kit (Cat# BMS6015; eBioscience; San Diego, CA, USA) according to manufacturer's instructions.

Statistical Analysis All data are presented as mean±standard error of the mean (SEM). Statistical analyses were performed using GraphPad Prism software (Version 9.1.1; GraphPad Software, San Diego, CA, USA). According to the normality of the data distribution, unpaired two-tailed Student's *t*-tests were used to compare CTL and RS groups. A P-value<0.05 was considered statistically significant. All histological and immunostaining assessments were performed in a blinded manner. Slides were coded by one investigator prior to staining, and imaging and quantitative analyses were conducted by another investigator who was unaware of the group allocation.

RESULTS

Restraint Stress Promotes Corneal Barrier Disruption by Stimulating Production of MMPs RS protocol successfully induced depression-like behavior in mice, as confirmed by behavioral tests. The corneal epithelium, as the outermost layer of the cornea, not only supports metabolic homeostasis but also serves as a critical barrier against external insults. To assess the impact of RS on ocular surface homeostasis, Oregon

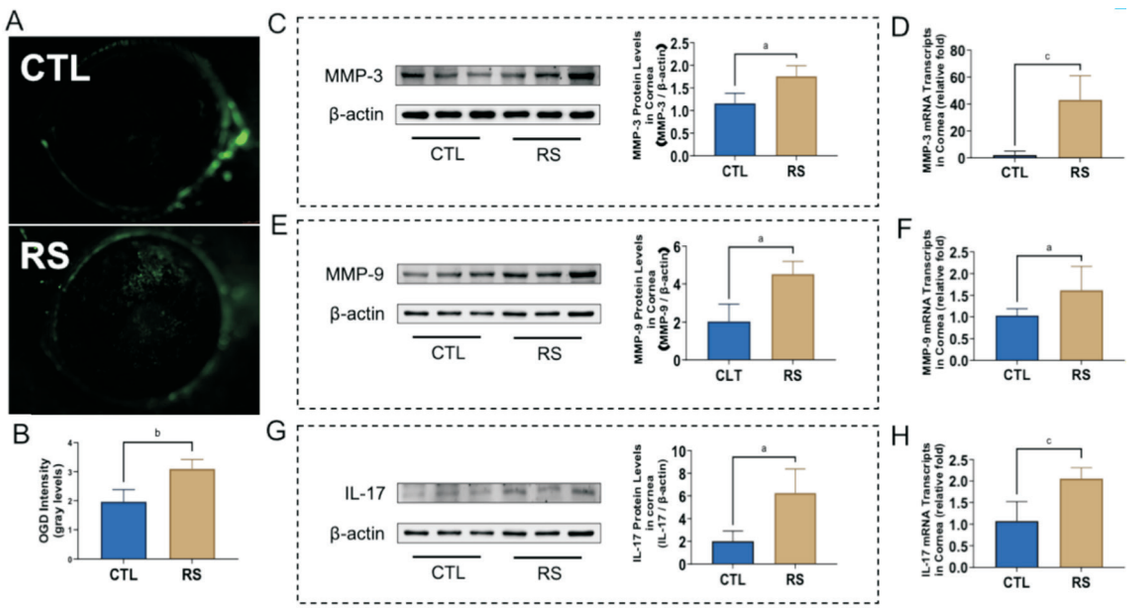

Figure 1 RS disrupts corneal epithelial barrier integrity and upregulates MMP-3, MMP-9, and IL-17 expression A: Representative images of Oregon Green Dextran (OGD) staining in mouse corneas; B: Quantification of corneal OGD fluorescence intensity; C, D: Protein and mRNA expression levels of MMP-3 in the cornea; E, F: Protein and mRNA expression levels of MMP-9 in the cornea; G, H: Protein and mRNA expression levels of IL-17 in the cornea. Data are presented as mean±SEM (n=6 mice per group). [a]P<0.05, [b]P<0.01, [c]P<0.001 *vs* control group. CTL: Control; RS: Restraint stress; MMP-3: Matrix metalloproteinase 3; MMP-9: Matrix metalloproteinase 9; IL-17: Interleukin 17; SEM: Standard error of the mean.

Green Dextran (OGD) uptake was performed to evaluate corneal epithelial barrier integrity. As shown in Figure 1A, 1B, mice subjected to RS exhibited significantly increased corneal OGD staining, indicative of epithelial barrier disruption. Previous studies have reported that IL-17, predominantly secreted by Th17 cells, stimulates the production of MMPs, especially MMP-3 and MMP-9, which contribute to corneal barrier breakdown[14]. Blocking IL-17 signaling decreases MMP expression and maintains corneal barrier function[15]. Consistent with these findings, our results demonstrated that the expression levels of IL-17, MMP-3, and MMP-9 in the cornea were significantly elevated in the RS group compared to controls (Figure 1C–1H).

Restraint Stress Induces Goblet Cells Loss *via* Imbalance in IFN-γ/IL-13 Axis To investigate the effect of RS on conjunctival goblet cell homeostasis, we quantified goblet cells using PAS staining. The results showed a significant reduction in goblet cell numbers in RS-treated mice (Figure 2A, 2B). Prior studies have demonstrated that the differentiation and maintenance of conjunctival goblet cells are regulated by the balance between Th1- and Th2-derived cytokines, notably IFN-γ and IL-13, respectively[16-18]. We hypothesized that RS-induced goblet cell loss might be associated with a dysregulated Th cytokine profile. Consistent with this, both gene and protein expression levels of IL-13 were markedly decreased, while those of IFN-γ were significantly increased in the conjunctiva of RS-treated mice compared to controls (Figure 2C–2F).

RS Induces Apoptosis of Ocular Surface Cells Apoptotic cell death serves as a pivotal pathophysiological mechanism in the development and progression of ocular surface disorders, notably DED[19-20]. In addition, activation of the caspase-dependent apoptotic pathway has been implicated in goblet cell loss[21-22]. To determine whether this pathway was involved in RS-induced ocular surface damage, we examined the expression of cleavedcaspase-3 and cleaved caspase-8 in the conjunctival epithelium using immunofluorescence and Western blot analysis. The results demonstrated a significant upregulation of both cleaved caspase-3 and cleaved caspase-8 in the conjunctiva of RS-treated mice compared to controls (Figure 3), suggesting the involvement of apoptosis in ocular surface damage under stress conditions.

Restraint Stress Induces Mild Inflammatory Changes in Lacrimal Gland Without Affecting Tear Production To determine whether ocular surface alterations in RS-treated mice were associated with changes in lacrimal gland function, we evaluated the gland's morphology, weight, and tear secretion. As shown in Figure 4A–4C, no significant differences were observed in lacrimal gland size, weight, or tear production between the RS and control groups. However, H&E staining revealed mild pathological changes in the lacrimal glands of RS-treated mice, characterized by acinar atrophy and inflammatory cell infiltration (Figure 4D). These features are suggestive of a stress-induced inflammatory response, although further immunophenotyping would be required to confirm the nature of the infiltrating immune cells.

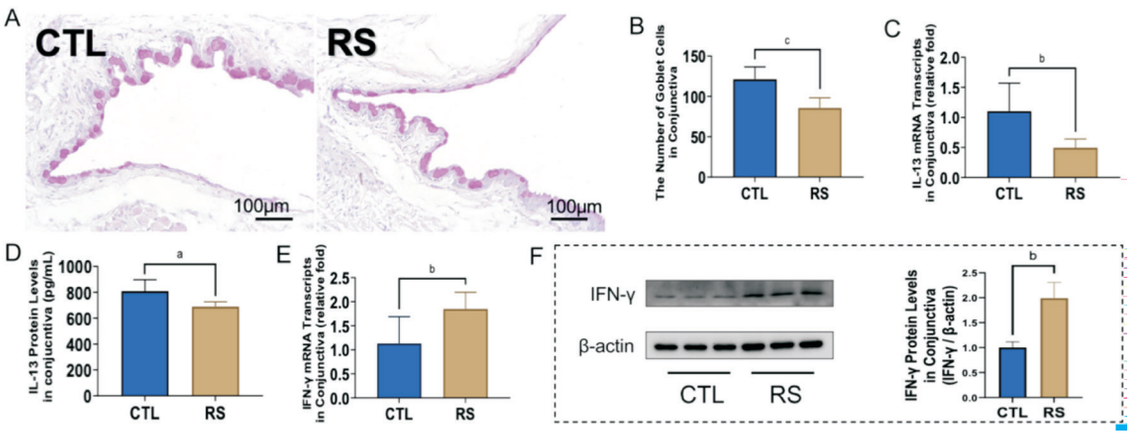

Figure 2 RS leads to conjunctival goblet cell loss through dysregulation of the IFN-γ/IL-13 axis A: Representative images of periodic acid-Schiff (PAS) staining showing conjunctival goblet cells in control and RS-treated mice (10×, scale bar: 100 μm); B: Quantification of goblet cell density per millimeter of conjunctival epithelium; C, D: mRNA and protein expression levels of IL-13 in the conjunctiva; IL-13 protein levels were determined by ELISA (pg/mL); E, F: mRNA and protein expression levels of IFN-γ in the conjunctiva; Data are presented as mean±SEM (n=6 mice per group). [a]P<0.05, [b]P<0.01, [c]P<0.001 *vs* control group. CTL: Control; RS: Restraint stress; IL-13: Interleukin 13; IFN-γ: Interferon gamma; SEM: Standard error of the mean.

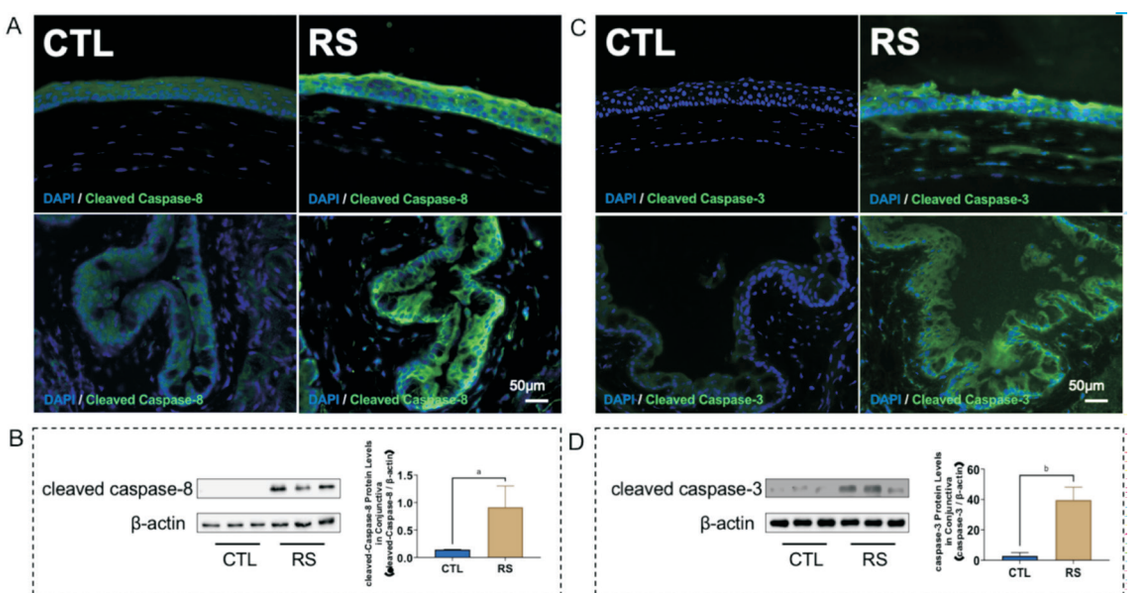

Figure 3 RS increases apoptosis in the ocular surface epithelium A: Representative immunofluorescence images showing cleaved caspase-8 expression in the corneal and conjunctival epithelium (20×, scale bar: 100 μm); B: Western blot analysis of cleaved caspase-8 protein levels in the conjunctiva; C: Representative immunofluorescence images showing cleaved caspase-3 expression in the corneal and conjunctival epithelium (20×, scale bar: 100 μm); D: Western blot analysis of cleaved caspase-3 protein levels in the conjunctiva. Data are presented as mean±SEM (n=6 mice per group). [a]P<0.05, [b]P<0.01 *vs* control group. CTL: Control; RS: Restraint stress; SEM: Standard error of the mean.

DISCUSSION

In this study, we demonstrate that RS-induced depressive-like behavior in mice leads to significant ocular surface alterations characteristic of DED. These changes include corneal epithelial barrier disruption, conjunctival goblet cell loss, and increased apoptosis in ocular surface epithelial cells. Importantly, these pathological features occurred in the absence of decreased tear production, suggesting that immune-mediated epithelial damage, rather than aqueous tear deficiency, plays a central role in the ocular phenotype observed under stress conditions.

Previous studies have consistently shown that depression is more strongly associated with dry eye symptoms than with objective clinical signs[7,23]. Notably, while antidepressant use has been suggested as a potential contributor to DED in patients with depression[24-26], several reports have shown that newly diagnosed, treatment-naive depression patients also present with ocular surface abnormalities, including reduced tear stability and increased staining scores[5], similar to findings in our study. The RS model used in our research, which excludes pharmacological interference, strengthens the

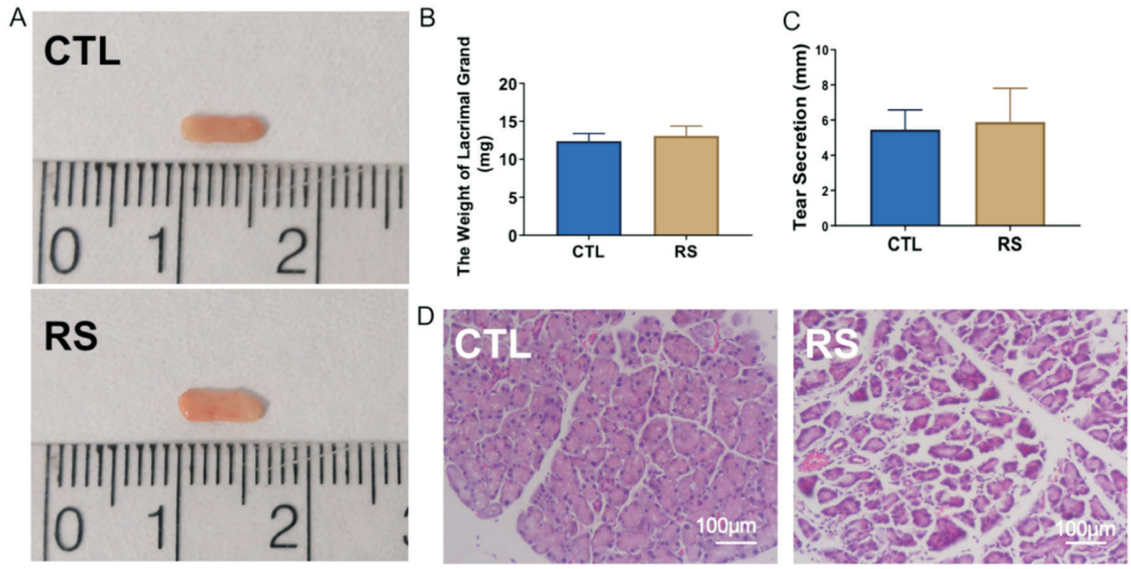

Figure 4 RS induces mild histological alterations in the lacrimal gland without affecting gland size or tear secretion A: Gross appearance of lacrimal glands from control and RS-treated mice; B: Comparison of lacrimal gland weight between groups; C: Quantification of tear secretion; D: Representative hematoxylin and eosin (H&E) staining of lacrimal glands showing focal mononuclear cell infiltration and mild tissue disorganization in RS-treated mice (scale bar: 100 μm). Data are presented as mean±SEM (*n*=7 mice per group). CTL: Control; RS: Restraint stress; SEM: Standard error of the mean.

hypothesis that depression itself can induce ocular surface pathology through immune modulation, independent of antidepressant therapy. Clinically, these observations align with findings that drug-naive patients with major depressive disorder exhibit compromised tear stability and elevated corneal staining compared to healthy controls, underscoring that depression-related immune dysregulation plays a central role in the observed ocular surface inflammation.

Mechanistically, we identified an imbalance in local immune mediators, characterized by elevated expression of pro-inflammatory cytokines IL-17 and IFN-γ and reduced levels of the protective Th2 cytokine IL-13. This disrupted cytokine profile is known to impair goblet cell differentiation and survival, enhance epithelial apoptosis, and upregulate MMPs, particularly MMP-3 and MMP-9[14,16,27]. These enzymes degrade corneal epithelial tight junctions and extracellular matrix components, contributing to barrier breakdown. Our data thus support a model in which depression-induced immune dysregulation promotes ocular surface damage through inflammatory cytokine cascades and proteolytic activity.

Interestingly, despite significant epithelial injury, tear production and gross lacrimal gland morphology remained largely unaffected. However, histological analysis revealed mild acinar atrophy and inflammatory cell infiltration, indicating subclinical inflammation. These findings suggest that lacrimal gland involvement may occur as a secondary response to immune activation, potentially exacerbating ocular surface damage over time[28-29].

This study has several limitations. The RS model used in this study reliably induces depression-like behaviors and has been widely employed in related research. Nevertheless, as an acute stress paradigm, it may also evoke systemic stress responses in addition to behavioral changes. Therefore, the ocular surface alterations observed here are likely influenced by both behavioral and physiological factors. Although this model effectively reproduces key features of stress-related ocular changes, it may not fully reflect the chronic and multifactorial nature of human depression. Future studies employing alternative or longer-term stress paradigms could help further delineate the contributions of specific stress components[30]. In addition, the sample size in certain experiments was relatively small, and further studies with larger cohorts are warranted to confirm these findings. Finally, while cytokine imbalance and MMP activation were observed, the specific immune pathways remain unclear. Future studies using immune profiling and targeted interventions will be needed to clarify the mechanisms linking depression to ocular surface inflammation.

This study demonstrates that depression-like stress induces dry eye-like changes in mice, including corneal barrier disruption, goblet cell loss, and epithelial apoptosis. These alterations occur without reduced tear production and are associated with an imbalance of ocular surface cytokines. Our findings suggest that depression may contribute to ocular surface inflammation *via* immune-mediated pathways, providing a potential mechanistic link between mental health and dry eye disease.

ACKNOWLEDGEMENTS

Authors' Contributions: Lin X: Conceptualization, funding

acquisition, investigation, formal analysis, data curation, methodology, writing-original draft, writing-review & editing. Liu YW: Conceptualization, formal analysis, data curation, methodology, writing-original draft, writing-review & editing. Li JN: Formal analysis, data curation, methodology, writing-original draft, writing-review & editing. Ouyang WJ: Conceptualization, methodology, writing-review & editing. Tang LY: Conceptualization, methodology, writing-review & editing. Wu JL: Conceptualization, methodology, writing-review & editing. Liu ZL: Conceptualization, methodology, writing-review & editing. Wu SN: Conceptualization, methodology, writing-review & editing. Hu JY: Conceptualization, supervision, funding acquisition, writing-review & editing. Liu ZG: Conceptualization, supervision, funding acquisition, writing-review & editing.

Data Availability: The data are available from the corresponding author, Liu ZG (zuguoliu@xmu.edu.cn), upon reasonable request.

Foundations: Supported by the Key Program of the National Natural Science Foundation of China (No.82530034); the National Natural Science Foundation of China (No.82271054); the Nature Science Foundation of Xiamen, China (No.3502Z20227121).

Conflicts of Interest: Lin X, None; **Liu YW,** None; **Li JN,** None; **Ouyang WJ,** None; **Tang LY,** None; **Wu JL,** None; **Liu ZL,** None; **Wu SN,** None; **Hu JY,** None; **Liu ZG,** None.

REFERENCES

1 Global Health Data Exchange (GHDx). 2023. https://vizhub.healthdata.org/gbd-results/ (accessed on 4 March 2023).

2 GBD 2021 Diseases and Injuries Collaborators. Global incidence, prevalence, years lived with disability (YLDs), disability-adjusted life-years (DALYs), and healthy life expectancy (HALE) for 371 diseases and injuries in 204 countries and territories and 811 subnational locations, 1990-2021: a systematic analysis for the Global Burden of Disease Study 2021. *Lancet* 2024;403(10440):2133-2161.

3 Tang WSW, Lau NXM, Krishnan MN, *et al*. Depression and eye disease-a narrative review of common underlying pathophysiological mechanisms and their potential applications. *J Clin Med* 2024;13(11):3081.

4 Craig JP, Nichols KK, Akpek EK, *et al*. TFOS DEWS II definition and classification report. *Ocul Surf* 2017;15(3):276-283.

5 Wolffsohn JS, Benítez-Del-Castillo JM, Loya-Garcia D, *et al*. TFOS DEWS III: diagnostic methodology. *Am J Ophthalmol* 2025;279:387-450.

6 Zheng Y, Wu X, Lin X, *et al*. The prevalence of depression and depressive symptoms among eye disease patients: a systematic review and meta-analysis. *Sci Rep* 2017;7:46453.

7 Zhou Y, Murrough J, Yu Y, *et al*. Association between depression and severity of dry eye symptoms, signs, and inflammatory markers in the DREAM study. *JAMA Ophthalmol* 2022;140(4):392.

8 Ulusoy MO, Işık-Ulusoy S, Kıvanç SA. Evaluation of dry eye disease in newly diagnosed anxiety and depression patients using anterior segment optical coherence tomography. *Eye Vis* (*Lond*) 2019;6:25.

9 Tiskaoglu NS, Yazıcı A, Karlıdere T, *et al*. Dry eye disease in patients with newly diagnosed depressive disorder. *Curr Eye Res* 2017;42(5):672-676.

10 Gökçe GD, Metin M. Is there a relationship between the severity of disease in major depressive disorder patients and dry eye disease? *Int Ophthalmol* 2024;44(1):163.

11 Chu X, Zhou Y, Hu Z, *et al*. 24-hour-restraint stress induces long-term depressive-like phenotypes in mice. *Sci Rep* 2016;6:32935.

12 Li Z, Chen K, Shao Q, *et al*. Nanoparticulate MgH_2 ameliorates anxiety/depression-like behaviors in a mouse model of multiple sclerosis by regulating microglial polarization and oxidative stress. *J Neuroinflammation* 2023;20(1):16.

13 Liu Z, Yang Y, Yan K, *et al*. Light-emitting diode-derived blue light overexposure accelerates corneal endothelial cell aging by inducing abnormal ROS accumulation. *J Photochem Photobiol B Biol* 2025;272:113252.

14 Vereertbrugghen A, Pizzano M, Cernutto A, *et al*. $CD4^+$T cells drive corneal nerve damage but not epitheliopathy in an acute aqueous-deficient dry eye model. *Proc Natl Acad Sci U S A* 2024;121(48):e2407648121.

15 Huang D, Li Z. Multidimensional immunotherapy for dry eye disease: current status and future directions. *Front Ophthalmol* 2024;4:1449283.

16 Alam J, de Paiva CS, Pflugfelder SC. Immune - Goblet cell interaction in the conjunctiva. *Ocul Surf* 2020;18(2):326-334.

17 Coursey TG, Tukler Henriksson J, Barbosa FL, *et al*. Interferon-γ-induced unfolded protein response in conjunctival goblet cells as a cause of mucin deficiency in sjögren syndrome. *Am J Pathol* 2016;186(6):1547-1558.

18 Lin N, Chen X, Liu H, *et al*. Ectoine enhances mucin production *via* restoring IL-13/IFN-γ balance in a murine dry eye model. *Invest Ophthalmol Vis Sci* 2024;65(6):39.

19 Li J, Bao X, Guo S, *et al*. Cell death pathways in dry eye disease: Insights into ocular surface inflammation. *Ocul Surf* 2024;34:535-544.

20 Scarpellini C, Ramos Llorca A, Lanthier C, *et al*. The potential role of regulated cell death in dry eye diseases and ocular surface dysfunction. *Int J Mol Sci* 2023;24(1):731.

21 de Paiva CS, Trujillo-Vargas CM, Schaefer L, *et al*. Differentially expressed gene pathways in the conjunctiva of sjögren syndrome keratoconjunctivitis sicca. *Front Immunol* 2021;12:702755.

22 Contreras-Ruiz L, Ghosh-Mitra A, Shatos MA, *et al*. Modulation of conjunctival goblet cell function by inflammatory cytokines. *Mediators Inflamm* 2013;2013:636812.

23 Stapleton F, Argüeso P, Asbell P, *et al*. TFOS DEWS III: digest. *Am J Ophthalmol* 2025;279:451-553.

24 Işik-Ulusoy S, Ulusoy MO. Influence of different antidepressants on ocular surface in patients with major depressive disorder. *J Clin Psychopharmacol* 2021;41(1):49-52.

25 Ismayilov AS, Celikel G. Effects of tricyclic antidepressants, selective serotonin reuptake inhibitors, and selective serotonin-norepinephrine reuptake inhibitors on the ocular surface. *Arq Bras Oftalmol* 2022;86(5):e20230068.

26 Mansoor A, Mansoor S, Khan AH. Antidepressants and ocular health: Addressing dry eye syndrome. *J Shifa Tameer E Millat Univ* 2024;7(1):86-94.

27 Zhang Y, Yang M, Zhao SX, *et al*. Hyperosmolarity disrupts tight junction *via* TNF-α/MMP pathway in primary human corneal epithelial cells. *Int J Ophthalmol* 2022;15(5):683-689.

28 Bron AJ, de Paiva CS, Chauhan SK, *et al*. TFOS DEWS II pathophysiology report. *Ocul Surf* 2017;15(3):438-510.

29 de Paiva CS, St Leger AJ, Caspi RR. Mucosal immunology of the ocular surface. *Mucosal Immunol* 2022;15(6):1143-1157.

30 Xie M, Long H, Tian S, *et al*. Saikosaponin F ameliorates depression-associated dry eye disease by inhibiting TRIM8-induced TAK1 ubiquitination. *Int Immunopharmacol* 2024;130:111749.